

## SCIENTIFIC AND TECHNICAL SECTION

### CONDITIONS FOR THE TRANSITION FROM NONLOCALIZED TO LOCALIZED DAMAGE IN METALS AND ALLOYS. PART 3. DETERMINATION OF THE TRANSITION CONDITIONS BY THE ANALYSIS OF CRACK PROPAGATION KINETICS

V. T. Troshchenko and L. A. Khamaza

UDC 539.421

*Special features of initiation and growth of short cracks under stresses above the fatigue limit are studied for a wide range of metals and alloys. The authors analyze the growth kinetics of short fatigue cracks, which is assessed by the dependence of crack length or crack growth rate on the number of loading cycles. The transition from the stage of short crack propagation (nonlocalized fatigue damage) to the stage of a main crack propagation (localized fatigue damage) is shown to be characterized by a more intensive increase of the crack growth rate. A procedure for determination of the main crack sizes corresponding to the transition from nonlocalized to localized fatigue damage has been substantiated. It has been found out that the fatigue crack sizes corresponding to this transition at stresses above the fatigue limit decrease with increasing stresses and remain smaller than those at stresses equal to the fatigue limit.*

**Keywords:** fatigue, main crack, nonlocalized and localized damage.

**Introduction.** In the process of cyclic loading of metals and alloys with stresses above the fatigue limit, there arise numerous of fatigue microcracks. During the further loading some cracks stop growing, while the others keep on propagating with a low rate and only one crack (or a few of them), having reached a certain size, starts growing with a high rate resulting in the ultimate failure of the structural element. This crack is called the main fatigue crack. The process of its propagation can be subdivided into two stages.

During the first stage the crack does not differ from many others in size or growth rate. We will call it the stage of nonlocalized fatigue damage.

At the second stage the crack, for some reasons not to be discussed here, starts propagating with a high rate and the further process of fatigue fracture of the structural element is governed by the propagation of this crack. It is during this stage that the fatigue crack exhibits the properties which give reason to name it the main crack. The fatigue crack growth stage will be referred to as the localized fatigue damage stage.

Of interest is to analyze conditions for the transition of the main crack from the nonlocalized to localized fatigue damage. The conditions for the transition are taken to mean primarily the fatigue crack sizes and the number of cycles of loading till this transition.

Upon transition from one fatigue crack growth stage to the other, of interest is to clarify the possibility of determining the transition conditions on the basis of the analysis of the crack growth kinetics within the range of the number of cycles corresponding to this transition.

---

Pisarenko Institute of Problems of Strength, National Academy of Sciences of Ukraine, Kiev, Ukraine. Translated from Problemy Prochnosti, No. 5, pp. 5 – 19, September – October, 2014. Original article submitted November 25, 2013.

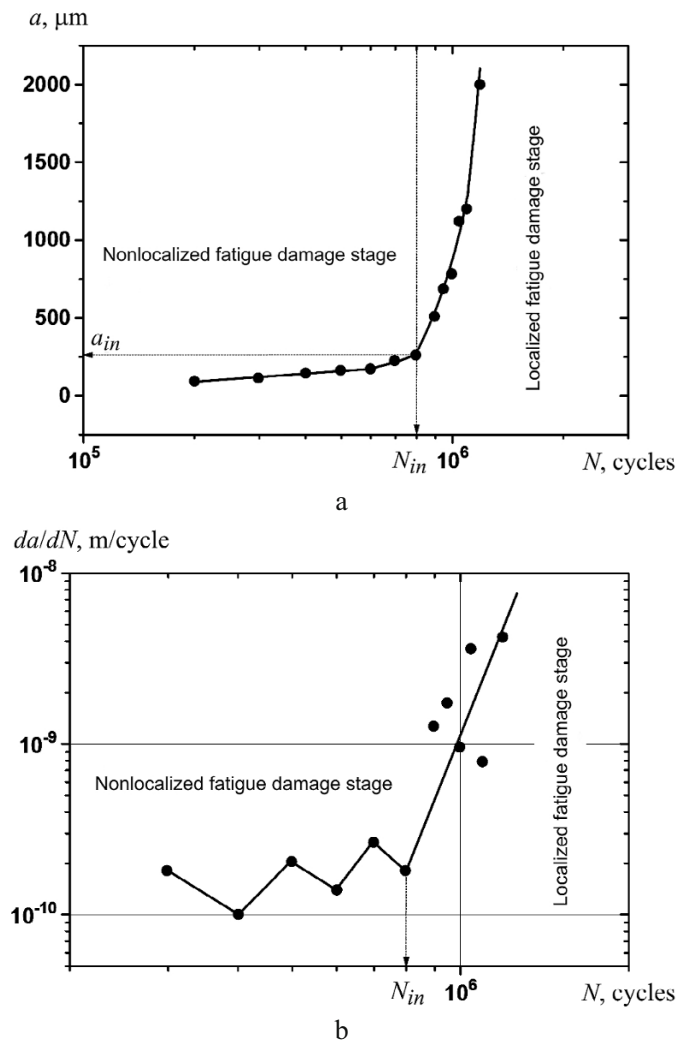


Fig. 1. Crack depth (a) and crack growth rate (b) versus the number of loading cycles for austenitic stainless steel 316L ( $\epsilon_{ap} = 3 \cdot 10^{-5}$ , number of cycles to failure  $N_f = 1.19 \cdot 10^6$ ,  $N_{in} = 8 \cdot 10^5$  cycles, and  $a_{in} = 257 \mu\text{m}$ ).

The available publications provide a great body of experimental data on the fatigue crack growth kinetics; however, many researchers address the crack propagation starting from the sizes above the value corresponding to the transition from nonlocalized to localized fatigue damage.

Here, we will discuss the available findings [1–22] of investigations of the fatigue crack growth kinetics, starting from very small crack sizes, put forward and substantiate the method for determination of conditions for the transition from nonlocalized to localized fatigue damage based on the analysis of the fatigue crack growth rate variations under cyclic loading.

**The Method for Determination of Conditions for the Transition from Nonlocalized to Localized Fatigue Damage.** Figure 1 illustrates the dependence of the crack depth  $a$  and crack growth rate  $da/dN$  on the number of loading cycles  $N$  for austenitic stainless steel 316L under testing with a constant plastic strain amplitude  $\epsilon_{ap}$  [7, 17, 18]. One can see two distinct segments in the diagrams. At the first one the crack size and growth rate are small and vary insignificantly with the number of loading cycles, while at the second segment they rise sharply. Therefore, the crack size  $a_{in}$  and the number of cycles  $N_{in}$  can be taken as the characteristics corresponding to the transition from nonlocalized to localized fatigue damage. Figure 1a clearly shows that the fatigue crack behavior is different at the stages of nonlocalized and localized fatigue damage, which is not always the case.

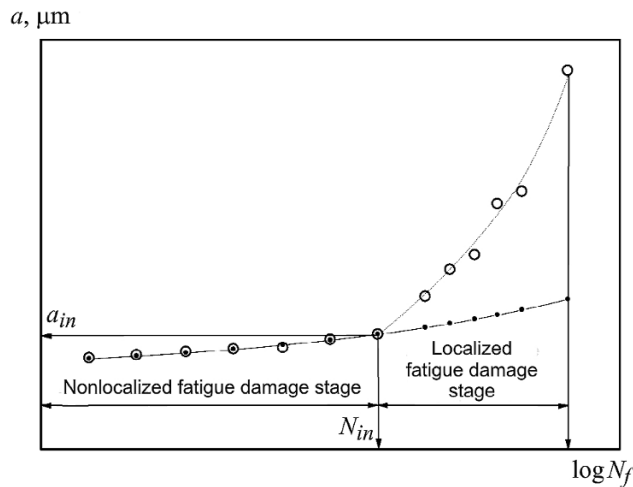


Fig. 2. Schematic representation of the crack propagation: (○) experimental data; (●)  $a = a_0 \exp[\ln(a_{in}/a_0) N/N_{in}]$ .

Analysis of experimental data on the fatigue crack growth kinetics from the instant of the crack initiation till the ultimate failure suggests that it is impossible to describe the dependence of the crack length on the number of loading cycles by a single exponential, transcendental, or power function as proposed in [9, 14, 18, 20].

Generally, at an early stage of its propagation the crack is described by the exponential law [2]. As the crack size reaches the value  $a = a_{in}$  the dependence of the crack depth on the number of cycles departs from the initial exponential law.

This special feature associated with a change of the function dependence of the crack growth  $a = f(N)$  is proposed to be used for determination of the crack size  $a_{in}$  and the related number of loading cycles  $N_{in}$ , which is done in the following way.

The dependence of the crack depth  $a$  on the number of cycles  $N$  at an early stage of the crack propagation is described by the equation

$$a = a_0 \exp(kN_i), \quad (1)$$

where the coefficient  $k$  is the crack length increment per cycle; the parameter  $a_0$  is the extrapolated value of the crack length to the number of cycles  $N_i = 0$ .

The crack size during the transition from one stage of fracture to the other is given by

$$a_{in} = a_0 \exp(kN_{in}), \quad (2)$$

hence we have

$$k = \frac{\ln(a_{in}/a_0)}{N_{in}}. \quad (3)$$

Substitution of (3) into (1) gives

$$a = a_0 \exp \left[ \ln(a_{in}/a_0) \frac{N_i}{N_{in}} \right]. \quad (4)$$

By successively substituting the current experimental values of the crack size  $a_i$  and the corresponding numbers of cycles  $N_i$  into relation (4) and selecting the parameter  $a_0$  we achieve the best description of experimental data by this relation for the stage of nonlocalized fatigue damage (Fig. 2). The values of  $a_i$  and  $N_i$  that satisfy this condition and whereby the experimental data depart from the exponential function will in fact represent the critical values of the crack size  $a_{in}$  and lifetime  $N_{in}$  corresponding to the transition from nonlocalized to localized fatigue damage.

If the dependence of the crack length  $a$  on the number of loading cycles  $N_i$  is assumed to obey the exponential law over the entire lifetime range till failure, Eq. (4) is written as

$$a = a_i \exp \left[ \ln(a_f/a_i) \frac{N_i}{N_f} \right], \quad (5)$$

where  $a_i$  is the crack size corresponding to the size of an element of the material structure (ferrite grain, bainite and martensite platelets, inclusions, and so on), and  $a_f$  is the crack size at failure.

The use of Manson–Coffin equations for tension–compression and torsion

$$\varepsilon_{ap} = \varepsilon'_f (N_f)^c,$$

$$\gamma_{ap} = \gamma'_f (N_f)^{c'},$$

where  $\varepsilon_{ap}$  and  $\gamma_{ap}$  are the plastic strain amplitudes in tension–compression and torsion, respectively,  $\varepsilon'_f$  and  $\gamma'_f$  are cycle plasticity coefficients in tension–compression and torsion,  $c$  and  $c'$  are the cycle plasticity exponents in tension–compression and torsion, respectively, and  $N_f$  is the number of cycles to failure, leads to the following expressions relating the crack size to the number of cycles and plastic strain amplitude:

$$a = a_i \exp \left[ \ln(a_f/a_i) \left( \frac{\varepsilon_{ap}}{\varepsilon'_f} \right)^{-1/c} N_i \right], \quad (6)$$

$$a = a_i \exp \left[ \ln(a_f/a_i) \left( \frac{\gamma_{ap}}{\gamma'_f} \right)^{-1/c'} N_i \right]. \quad (7)$$

Using the Basquit equations for tension–compression and torsion

$$\sigma_a = \sigma'_f (N_f)^b,$$

$$\tau_a = \tau'_f (N_f)^{b'},$$

where  $\sigma_a$  and  $\tau_a$  are the stress amplitudes in tension–compression and torsion, respectively,  $\sigma'_f$  and  $\tau'_f$  are cycle strength coefficients in tension–compression and torsion,  $b$  and  $b'$  are the cycle strength exponents in tension–compression and torsion, respectively, we have the following expressions relating the crack size to the number of loading cycles and stress amplitude:

$$a = a_i \exp \left[ \ln(a_f/a_i) \left( \frac{\sigma_a}{\sigma'_f} \right)^{-1/b} N_i \right], \quad (8)$$

$$a = a_i \exp \left[ \ln(a_f/a_i) \left( \frac{\tau_a}{\tau'_f} \right)^{-1/b'} N_i \right]. \quad (9)$$

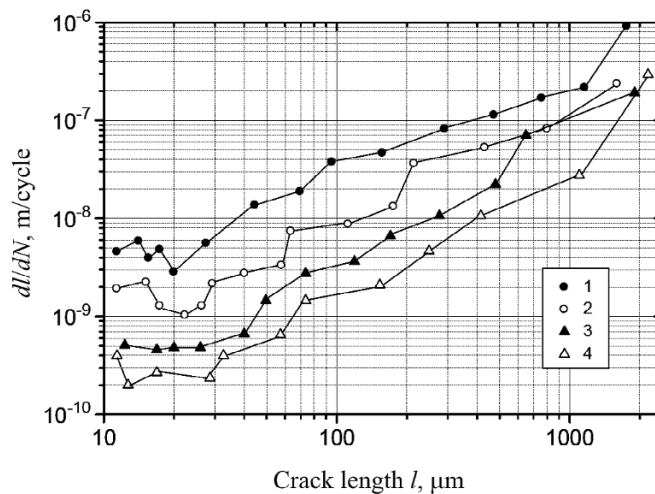


Fig. 3. The crack growth rate as a function of the crack length and stress level for a medium-carbon steel (0.43% C): (1)  $\sigma_a = 382$  MPa, (2)  $\sigma_a = 353$  MPa, (3)  $\sigma_a = 323$  MPa, and (4)  $\sigma_a = 304$  MPa.

Note that using Eqs. (6)–(9) and having available the fatigue curves corresponding to the ultimate failure of the specimen one can plot the fatigue curves of specimens and structural members, which will correspond to certain fixed crack sizes.

The transition to localized fatigue damage can be also defined by representing the experimental data on the crack growth kinetics in the form of the dependence of the crack growth rate  $da/dN$  on the number of loading cycles  $N$  (Fig. 1b). A typical feature of this function is the presence of a break point corresponding to the crack size  $a_{in}$  and lifetime  $N_{in}$ , whereupon the crack propagation becomes noticeably faster.

Noteworthy is that the methods outlined above should complement each other in order to improve reliability of determination of the main crack size.

**The Main Crack Size and the Number of Loading Cycles Corresponding to the Transition from Nonlocalized to Localized Fatigue Damage.** Zhixue [11] studied the growth kinetics of surface fatigue cracks in medium-carbon steel smooth specimens under rotational bending. The surface cracks were recorded and measured through the use of plastic replicas in uniform intervals till the specimen failure. The minimum noted crack size was approximately 10  $\mu\text{m}$ . The experimental data [11] are given in the form of the dependence of the surface crack growth rate on the crack length (Fig. 3). The tests were carried out at four stress levels (MPa): 382 ( $N_f = 2.36 \cdot 10^4$  cycles), 353 ( $N_f = 6.64 \cdot 10^4$  cycles), 323 ( $N_f = 2.18 \cdot 10^5$  cycles), and 304 ( $N_f = 5.1 \cdot 10^5$  cycles).

In Fig. 3 one can observe a transition to the intensive crack growth at all stress levels. However, this transition becomes more pronounced when the experimental data are represented as “crack growth rate-vs.-number of loading cycles” (Fig. 4).

Figure 4 shows break points in the  $dl/dN - N$  and lifetime  $N_{in}$  curves, which correspond to the transition from nonlocalized to localized fatigue damage.

The length of the main crack line corresponding to this transition can be found by using the dependence of the experimental crack length values on the number of cycles following the procedure as outlined in the previous section. The results of such determination for a medium-carbon steel (0.43% C) are given in Fig. 5.

Figure 6 shows the main crack length  $l_{in}$  as a function of the stress level for a medium-carbon steel (0.43% C).

The data given in Fig. 6 suggest that the main crack size corresponding to the transition from nonlocalized to localized fatigue damage is not constant but depends on the stress level. The higher the stress level, the smaller the crack size. At the stresses corresponding to the fatigue limit the crack size is maximum.

As shown above, the duration of the main crack initiation stage is assessed by the lifetime  $N_{in}$  that corresponds to the start of intensive crack growth.

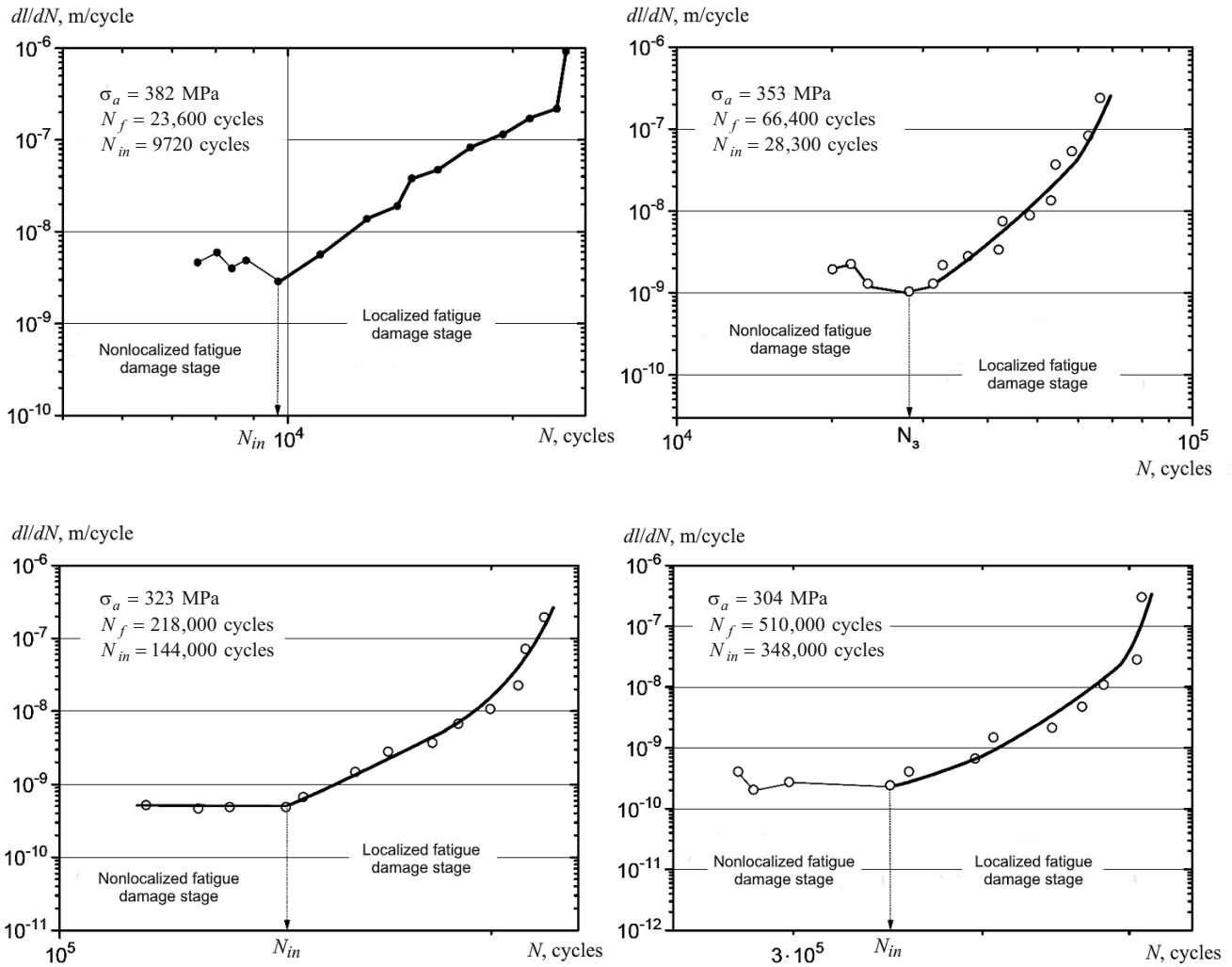


Fig. 4. The crack growth rate vs. the number of cycles at different stress levels for a medium-carbon steel (0.43% C).

Of interest is to compare the number of cycles till initiation of the main crack of size  $a_{in}$  and the number of cycles till initiation of a crack whose size is equal to that of an element of the material structure.

The crack growth rate can be expressed in terms of the linear fracture mechanics as follows:

$$\frac{da}{dN} = C(K_a)^m = C(Y\sigma_a \sqrt{\pi a})^m, \quad (10)$$

where  $K_a$  is the stress intensity factor,  $\sigma_a$  is the stress amplitude,  $C$  and  $m$  are the parameters of the kinetic fatigue fracture diagram in coordinates  $da/dN - K_a$ , and  $Y$  is the geometrical factor ( $Y = 0.65$  for a semicircular crack and  $Y = 1.12$  for a through crack).

The duration of the stage of initiation of a crack with a size equal to that of the material structural element  $d$  or to the inclusion size  $d_{incl}$  is given by

$$N_i = N_f - N_{fs},$$

where  $N_{fs}$  is the number of cycles whereby the crack grows from the size corresponding to that of the material structural element till the ultimate failure.

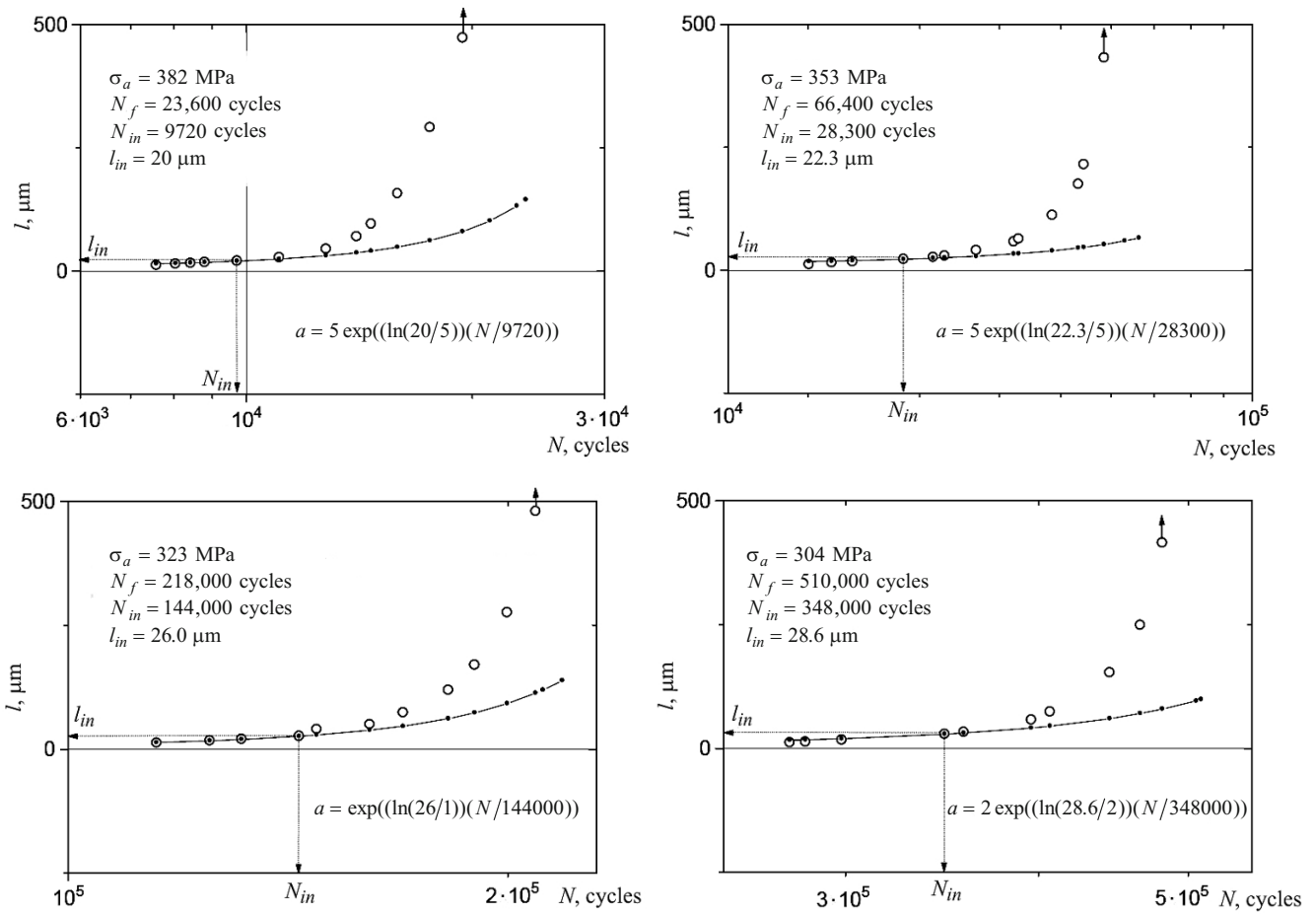


Fig. 5. Experimental (symbols) and exponential (lines) dependence of the crack length on the number of loading cycles.

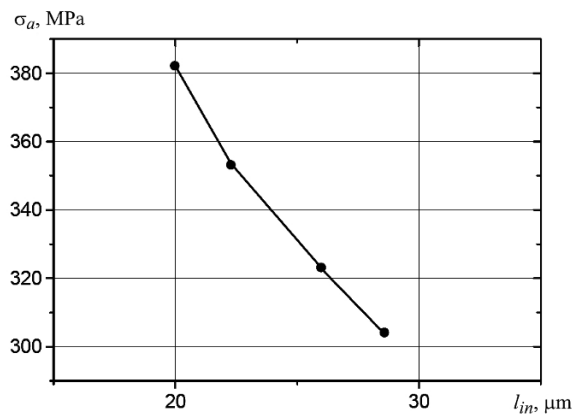


Fig. 6. The main crack length corresponding to the transition from nonlocalized to localized fatigue damage vs. the stress level for a medium-carbon steel (0.43% C).

The duration of the crack propagation stage  $N_{fs}$  can be computed by integrating Eq. (10):

$$N_{fs} = \int_{a_i}^{a_f} \frac{1}{C(Y\sigma_a \sqrt{\pi a})^m} da. \quad (11)$$

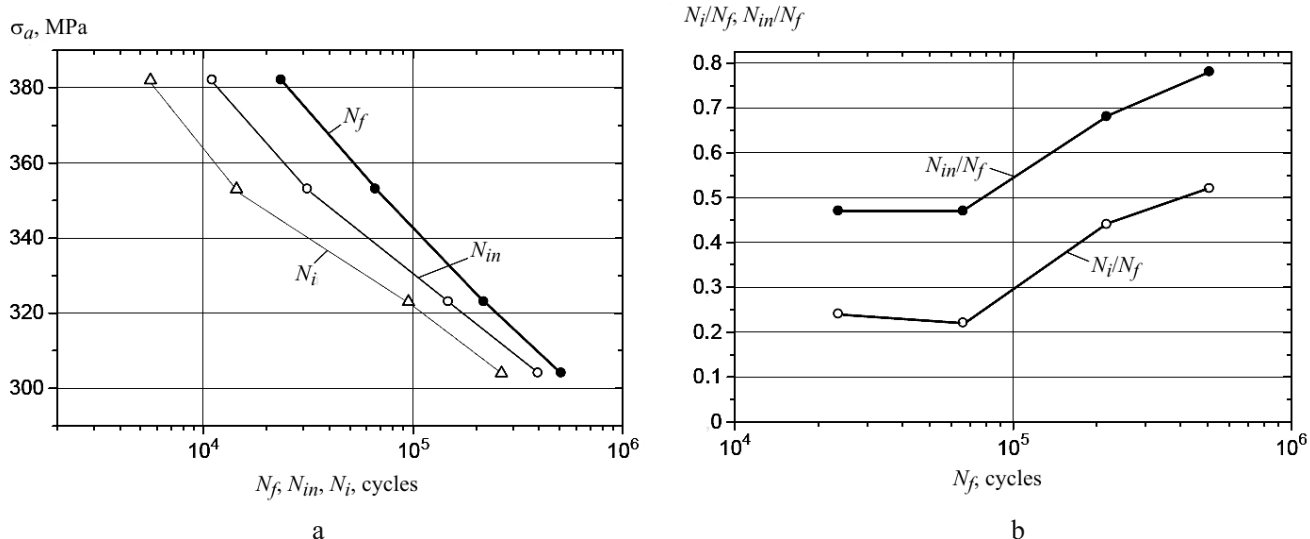


Fig. 7. Absolute (a) and relative life (b) till initiation of a structural and a main crack for a medium-carbon steel (0.43% C).

For further calculations by formula (11), the structural element size  $a_i$  and the crack size corresponding to the ultimate failure  $a_f$  were cited from the available publications.

Figure 7a shows fatigue curves for a medium-carbon steel (0.43% C), which were plotted for ultimate failure  $N_f$ , for structure crack propagation  $N_i$ , and for initiation of a main crack  $N_{in}$ . Figure 7b presents the curves of the relative duration of the structural crack propagation ( $N_i/N_f$ ) and the main crack initiation ( $N_{in}/N_f$ ). It is evident that the duration of these stages is not constant but increases with lifetime (with decreasing effective stresses). The relative duration of these stages grows to  $0.52N_f$  and  $0.78N_f$ , respectively.

The procedure for determination of the main crack size corresponding to the transition from nonlocalized to localized fatigue damage and for determination of the duration of crack initiation stage, which was outlined above for the case of a medium-carbon steel (0.43% C), was used for the study of crack growth kinetics in the following materials: aluminum alloy EN-AW 6082/T6 of two modifications [9], austenitic-ferritic steel SAF 2205 [14], steels Kh10CrAl24 [16], 42CrMo4 [20], SCr440 [22], and SCM435 [22], austenitic stainless steel 316L [18], and vacuum-annealed oxygen-free copper of purity 99.95% [6]. The results of these investigations, which are summarized in Table 1, demonstrate that the main crack size  $a_{in}$  varies over a wide range depending on the material class and load level: from 0.007–0.02 mm for carbon and alloy steels and aluminum alloy at the load levels corresponding to a small number of cycles till failure up to 0.74 mm for austenitic-ferritic steel at the loading levels corresponding to a large number of cycles to failure.

In the range of the number of cycles to failure  $10^5$ – $10^7$ , the main crack size  $a_{in}$  is 0.01–0.02 mm for carbon and alloy steels, 0.2–0.74 mm for high-ductile austenitic steels, and 0.155 mm for aluminum alloy.

Figure 8 illustrates the experimental dependence of the main crack size  $a_{in}$  on the number of cycles to failure  $N_f$  for all the materials studied.

It is obvious that, despite the fairly large discrepancy in absolute values of the main crack size between different classes of materials, the crack size corresponding to the transition from nonlocalized to localized fatigue damage is not constant for each particular material but depends on the stress level (the number of cycles to failure). The higher the level, the smaller the crack size. At the stresses corresponding to the fatigue limit the crack size is maximum.

For all the materials under consideration, the initiation of the main fatigue crack in smooth specimens under axial loading occurs, depending on the stress level, at a number of loading cycles equal to 0.4–0.86 of the number of cycles to failure, i.e., in this case, the stage of initiation of even very small fatigue cracks (0.01–0.05 mm) is equal to the major portion of the fatigue life.



TABLE 1. The Main Crack Sizes Corresponding to the Transition from Nonlocalized to Localized Fatigue Damage and Relative Durations of Crack Initiation Stages for Various Materials

Material	Specimen, loading mode	$\sigma_a$ , MPa ( $\varepsilon_{af}$ , mm/mm)	$N_f$ , cycles	$N_i$ , cycles	$N_{in}$ , cycles	$a_{in}$ , $\mu\text{m}$	$N_i/N_f$	$N_{in}/N_f$
1	2	3	4	5	6	7	8	9
Medium-carbon steel (0.43% C), ( $\sigma_u = 625$ MPa, $\sigma_Y = 375$ MPa, $d = 16.5$ $\mu\text{m}$ )	Smooth specimen, rotational bending, $\sigma_a = \text{const}$	382	$2.36 \cdot 10^4$	$5.6 \cdot 10^3$	$9.72 \cdot 10^3$	7.5	0.24	0.41
		353	$6.64 \cdot 10^4$	$1.44 \cdot 10^4$	$3.15 \cdot 10^4$	8.4	0.22	0.47
		323	$2.18 \cdot 10^5$	$9.5 \cdot 10^4$	$1.48 \cdot 10^5$	9.8	0.44	0.68
		304	$5.1 \cdot 10^5$	$2.64 \cdot 10^5$	$3.96 \cdot 10^5$	10.7	0.52	0.78
Aluminum alloy EN-AW 6082/T6 ( $\sigma_u = 354$ MPa, $\sigma_Y = 308$ MPa, $d_{incl} = 20$ $\mu\text{m}$ )	Smooth specimen, tension-compression (along the rolling direction), $\sigma_a = \text{const}$	300	$3.81 \cdot 10^3$	$2 \cdot 10^3$	$2 \cdot 10^3$	20.0	0.52	0.52
		250	$4.08 \cdot 10^4$	$2.2 \cdot 10^4$	$3.3 \cdot 10^4$	56.0	0.54	0.81
		200	$1.38 \cdot 10^5$	$9.4 \cdot 10^4$	$1.15 \cdot 10^5$	155.0	0.68	0.83
Aluminum alloy EN-AW 6082/T6 ( $\sigma_u = 330$ MPa, $\sigma_Y = 289$ MPa, $d_{incl} = 20$ $\mu\text{m}$ )	Smooth specimen, tension-compression (across the rolling direction), $\sigma_a = \text{const}$	300	$1.3 \cdot 10^3$	$0.4 \cdot 10^3$	$0.4 \cdot 10^3$	28.7	0.31	0.32
		250	$1.67 \cdot 10^4$	$8.7 \cdot 10^3$	$9.04 \cdot 10^3$	44.0	0.52	0.54
		200	$8 \cdot 10^4$	$5.95 \cdot 10^4$	$6.5 \cdot 10^4$	66.0	0.74	0.81
Austenitic-ferritic steel SAF 2205 ( $d = 20$ $\mu\text{m}$ )	Smooth specimen, tension-compression, $\varepsilon_{af} = \text{const}$	$(5 \cdot 10^{-3})$	$1.66 \cdot 10^3$	–	$6.28 \cdot 10^2$	108.0	–	0.38
		$(2 \cdot 10^{-3})$	$4.2 \cdot 10^3$	–	$2.29 \cdot 10^3$	75.6	–	0.55
		$(1 \cdot 10^{-3})$	$1.02 \cdot 10^4$	–	$6.17 \cdot 10^3$	193.0	–	0.60
		$(2 \cdot 10^{-4})$	$1.28 \cdot 10^5$	–	$1.06 \cdot 10^5$	430.0	–	0.83
		$(1 \cdot 10^{-4})$	$1.65 \cdot 10^5$	–	$1.41 \cdot 10^5$	222.0	–	0.85
		$(5 \cdot 10^{-5})$	$2.73 \cdot 10^5$	–	$2.34 \cdot 10^5$	744.0	–	0.86
Steel X10CrAl24	Smooth specimen, tension-compression, $\varepsilon_{af} = \text{const}$	$(1 \cdot 10^{-3})$	$1.14 \cdot 10^4$	–	$5.38 \cdot 10^3$	–	–	0.47
		$(5 \cdot 10^{-4})$	$2.42 \cdot 10^4$	–	$1.35 \cdot 10^4$	53.0	–	0.56
		$(2 \cdot 10^{-4})$	$8.74 \cdot 10^4$	–	$4.37 \cdot 10^4$	50.0	–	0.50
		$(1 \cdot 10^{-4})$	$1.68 \cdot 10^5$	–	$9.01 \cdot 10^4$	57.0	–	0.54
		$(5 \cdot 10^{-5})$	$2.72 \cdot 10^5$	–	$1.6 \cdot 10^5$	70.0	–	0.59
Forged cast steel 42CrMo4	Smooth specimen, tension-compression, $\varepsilon_{af} = \text{const}$	$(7 \cdot 10^{-4})$	$2.01 \cdot 10^4$	–	$3.07 \cdot 10^3$	17.1	–	0.15
		$(5 \cdot 10^{-4})$	$3.6 \cdot 10^4$	–	$1.5 \cdot 10^4$	118.0	–	0.42
		$(2 \cdot 10^{-4})$	$6.5 \cdot 10^4$	–	$4.01 \cdot 10^4$	135.0	–	0.62
		$(1 \cdot 10^{-4})$	$9.97 \cdot 10^4$	–	$7.5 \cdot 10^4$	180.0	–	0.75
		$(7 \cdot 10^{-5})$	$2.81 \cdot 10^5$	–	$2.09 \cdot 10^5$	284.0	–	0.74
Austenitic stainless steel 316L ( $\sigma_u = 562$ MPa, $\sigma_Y = 262$ MPa, $d_{incl} = 100$ $\mu\text{m}$ )	Smooth specimen, tension-compression, $\varepsilon_{af} = \text{const}$	$(1 \cdot 10^{-3})$	–	–	–	90.0	–	–
		$(5 \cdot 10^{-4})$	–	–	–	119.0	–	–
		$(2 \cdot 10^{-4})$	–	–	–	169.0	–	–
		$(1 \cdot 10^{-4})$	$7.2 \cdot 10^5$	–	$3.411 \cdot 10^5$	198.0	–	0.47
		$(5 \cdot 10^{-5})$	–	–	–	239.0	–	–
		$(3 \cdot 10^{-5})$	$1.103 \cdot 10^6$	–	$7.992 \cdot 10^5$	257.0	–	0.67
		$(3 \cdot 10^{-5})$	–	–	–	264.0	–	–
Annealed pure copper	Smooth specimen, tension-compression, $\varepsilon_{af} = \text{const}$	–	$8.85 \cdot 10^3$	–	$3.56 \cdot 10^3$	56.5	–	0.40
		–	$1.16 \cdot 10^5$	–	$6.1 \cdot 10^4$	162.0	–	0.53
Medium-carbon steel S45C ( $\sigma_u = 833$ MPa, $\sigma_Y = 750$ MPa, $\sigma_{-1} = 450$ MPa)	Smooth specimen, rotational bending, $\sigma_a = \text{const}$	700	$7.44 \cdot 10^3$	–	$2.076 \cdot 10^3$	8.8	–	0.28
		600	$3.38 \cdot 10^4$	–	$1.227 \cdot 10^4$	10.2	–	0.36
		500	$1.75 \cdot 10^5$	–	$6.685 \cdot 10^5$	14.1	–	0.38
		480	$2.71 \cdot 10^5$	–	$1.222 \cdot 10^5$	19.9	–	0.45

1	2	3	4	5	6	7	8	9
Steel SCr440 ( $\sigma_u = 994$ MPa, $\sigma_Y = 900$ MPa, $\sigma_{-1} = 500$ MPa)	Smooth specimen, rotational bending, $\sigma_a = \text{const}$	800	$1.09 \cdot 10^4$	–	$3.35 \cdot 10^3$	18.4	–	0.31
		750	$1.51 \cdot 10^4$	–	$7.13 \cdot 10^3$	30.2	–	0.47
		700	$2.42 \cdot 10^4$	–	$1.246 \cdot 10^4$	41.2	–	0.52
		520	$3.11 \cdot 10^5$	–	$2.034 \cdot 10^5$	72.0	–	0.65
Steel SCM435 ( $\sigma_u = 927$ MPa, $\sigma_Y = 832$ MPa, $\sigma_{-1} = 470$ MPa)	Smooth specimen, rotational bending, $\sigma_a = \text{const}$	800	$1.73 \cdot 10^4$	–	$6.64 \cdot 10^3$	39.0	–	0.38
		750	$2.09 \cdot 10^4$	–	$1.064 \cdot 10^4$	48.0	–	0.51
		700	$3.69 \cdot 10^4$	–	$1.99 \cdot 10^4$	52.0	–	0.54
		650	$6.31 \cdot 10^4$	–	$2.745 \cdot 10^4$	58.0	–	0.44
		600	$1.44 \cdot 10^5$	–	$7.95 \cdot 10^4$	60.0	–	0.55
		500	$3.98 \cdot 10^5$	–	$2.555 \cdot 10^5$	76.0	–	0.64

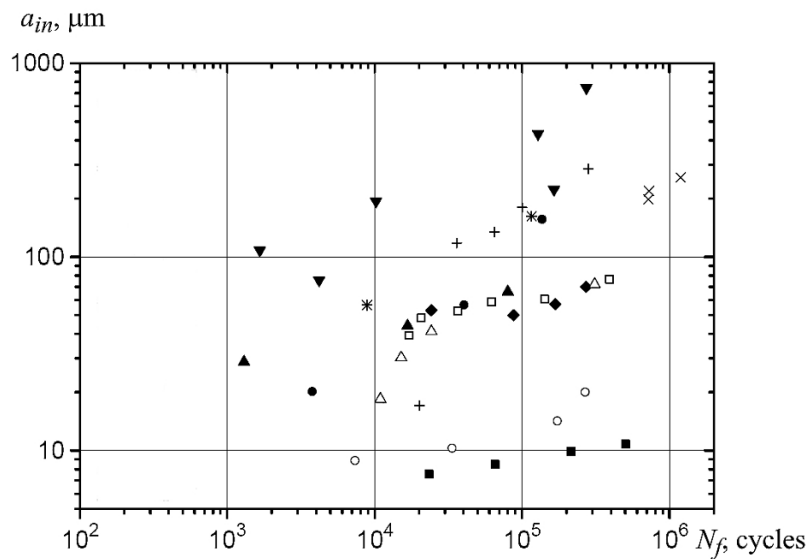


Fig. 8. The main crack size  $a_{in}$  as a function of the number of cycles to failure  $N_f$  for the materials studied. [Here and in Fig. 9: (■) medium-carbon steel, (●, ▲) aluminum alloy EN-AW 6082/T6 (along and across the rolling direction, respectively), (▼) austenitic-ferritic steel SAF 2205, (◆) steel X10CrAl24, (+) steel 42CrMo4, (×) austenitic steel 316L, (\*) annealed pure copper, (○, △, □) steels S45C, SCr440, and SCM435, respectively.]

Initiation of fatigue cracks whose size corresponds to the size of the structural element (a grain, secondary-phase particles, inclusions, and so on) takes place, depending on the effective stresses, in steel at  $(0.24\text{--}0.52)N_f$ , in aluminum alloy at  $(0.52\text{--}0.74)N_f$ , which also accounts for a significant portion of the total lifetime.

For the materials studied the ratio between the number of cycles to initiation of structural cracks  $N_i$  and the number of cycles to failure  $N_f$  and the ratio between the number of cycles to initiation of the main fatigue crack  $N_{in}$  and the number of cycles to failure  $N_f$  grow with increasing number of cycles failure.

Figure 9 shows the duration of main crack initiation stage ( $N_{in}/N_f$ ) as a function of the number of cycles to failure for the materials under consideration. It is evident that the duration of this stage is 30 to 80% of the total lifetime depending on the stress level (the number of cycles to failure).

**Conclusions.** The procedure for determination of the main crack size corresponding to the transition from nonlocalized to localized fatigue damage at stresses above the fatigue limit has been substantiated which is based on taking into account the variations of the functional dependence of the crack size and growth rate on the number of loading cycles.

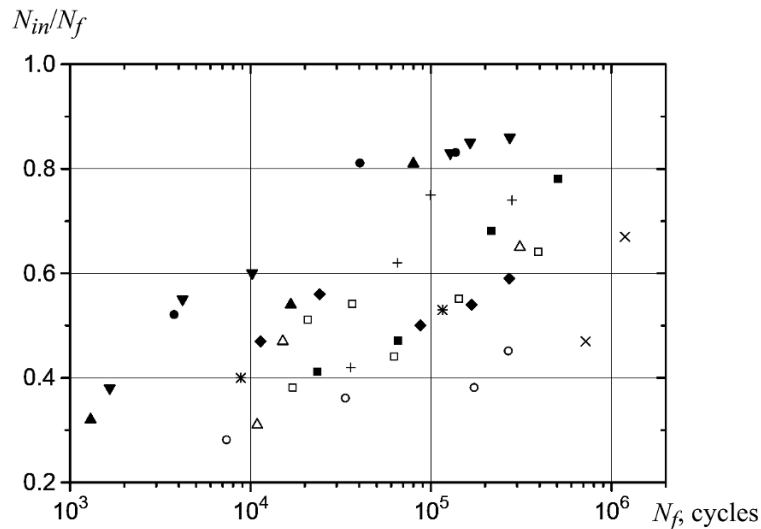


Fig. 9. Relative duration of the main crack initiation stage  $N_{in}/N_f$  vs. the number of cycles to failure  $N_f$ .

The fatigue crack sizes corresponding to the transition from nonlocalized to localized fatigue damage at stresses above the fatigue limit, which were determined from the dependences of the crack length and crack growth rate on the number of cycles, decrease with increasing stress and remain smaller, in comparison to those at the stresses equal to the fatigue limit.

## REFERENCES

1. C. Santus and D. Taylor, "Physically short crack propagation in metals during high cycle fatigue," *Int. J. Fatigue*, **31**, No. 8-9, 1356–1365 (2009).
2. Z. S. Basinski and S. J. Basinski, "Low amplitude fatigue of copper single crystals. – II. Surface observations. – III. PSB Sections," *Acta Met.*, **33**, 1307–1327 (1985).
3. J. Polák, T. Lepistö, and P. Kettunen, "Surface topography and crack initiation in emerging persistent slip bands in copper single crystals," *Mater. Sci. Eng.*, **74**, 85–91 (1985).
4. C. Blochwitz and D. Heinrich, "Microcrack propagation studies in fatigued nickel single crystals," in: P. Lukáš and J. Polák (Eds.), *Basic Mechanisms in Fatigue of Metals*, Elsevier, Amsterdam (1988), pp. 315–322.
5. J. Polák and P. Liškutín, "Nucleation and short growth in fatigued polycrystalline copper," *Fatigue Fract. Eng. Mater. Struct.*, **13**, No. 2, 119–133 (1990).
6. M. Chammouri, M. Abbadi, J. Mendez, et al., "An approach in plastic strain-controlled cumulative fatigue damage," *Int. J. Fatigue*, **33**, No. 2, 265–272 (2011).
7. A. Vašek and J. Polák, "Low cycle fatigue damage accumulation in armco-iron," *Fatigue Fract. Eng. Mater. Struct.*, **14**, No. 2-3, 193–204 (1991).
8. A. Plumtree and B. P. D. O'Connor, "Influence of microstructure on short fatigue crack growth," *Fatigue Fract. Eng. Mater. Struct.*, **14**, No. 2-3, 171–184 (1991).
9. D. Jiša, P. Liškutín, T. Krumpl, and J. Polák, "Small fatigue crack growth in aluminium EN-AW 6082/T6," *Int. J. Fatigue*, **32**, No. 12, 1913–1920 (2010).
10. M. Kage, K. J. Miller, and R. A. Smith, "Fatigue crack initiation and propagation in low-carbon steel of two different grain sizes," *Fatigue Fract. Eng. Mater. Struct.*, **15**, No. 8, 763–774 (1992).
11. W. Zhixue, "Short fatigue crack parameters describing the lifetime of unnotched steel specimens," *Int. J. Fatigue*, **23**, No. 4, 363–369 (2001).
12. C. M. Suh, R. Yuuki, and H. Kitagawa, "Fatigue microcracks in a low carbon steel," *Fatigue Fract. Eng. Mater. Struct.*, **8**, No. 2, 193–203 (1985).

13. A. Nasr, Y. Nadot, Ch. Bouraoui, et al., "Fatigue initiation in C35 steel: Influence of loading and defect," *Int. J. Fatigue*, **32**, No. 4, 780–787 (2010).
14. J. Polák and P. Zezulka, "Short crack growth and fatigue life in austenitic-ferritic duplex stainless steel," *Fatigue Fract. Eng. Mater. Struct.*, **28**, No. 10, 923–935 (2005).
15. F. Iacoviello, M. Boniardi, and G. M. La Vecchia, "Fatigue crack propagation in austeno-ferritic duplex stainless steel 22Cr5Ni," *Int. J. Fatigue*, **21**, No. 10, 957–963 (1999).
16. J. Polák, "Mechanisms and kinetics of the early fatigue damage in crystalline materials," *Mater. Sci. Eng. A*, **468-470**, 33–39 (2007).
17. A. Vašek, J. Polák, and K. Obrtlík, "Fatigue damage in two-step loading of 316L steel. II. Short crack growth," *Fatigue Fract. Eng. Mater. Struct.*, **19**, No. 2-3, 157–163 (1996).
18. K. Obrtlík, J. Polák, M. Hajek, and A. Vašek, "Short fatigue crack behaviour in 316L stainless steel," *Int. J. Fatigue*, **19**, No. 6, 471–475 (1997).
19. P. Hyspecky and B. Strnadel, "Conversion of short fatigue cracks into a long crack," *Fatigue Fract. Eng. Mater. Struct.*, **15**, No. 9, 845–854 (1992).
20. J. Polák, "Plastic strain-controlled short crack growth and fatigue life," *Int. J. Fatigue*, **27**, No. 10-12, 1192–1201 (2005).
21. X. Demulsant and J. Mendez, "Microstructural effects on small fatigue crack initiation and growth in Ti6Al4V alloys," *Fatigue Fract. Eng. Mater. Struct.*, **18**, No. 12, 1483–1497 (1995).
22. M. Goto and H. Nisitani, "Fatigue life prediction of heat-treated carbon steels and low alloy steels based on a small crack growth law," *Fatigue Fract. Eng. Mater. Struct.*, **17**, No. 2, 171–185 (1994).